

1 **A global analysis of reconstructed land climate changes during Dansgaard-** 2 **Oeschger events**

3 Mengmeng Liu^{1,2,*}, Iain Colin Prentice¹, Sandy P. Harrison²

4 1: Georgina Mace Centre for the Living Planet, Department of Life Sciences, Imperial College
5 London, Silwood Park Campus, Buckhurst Road, Ascot SL5 7PY, UK

6 2: Department of Geography and Environmental Science, University of Reading, Reading,
7 RG6 6AB, UK

8 *** Corresponding author: m.liu18@imperial.ac.uk**

9 Ms for: *Climate of the Past*

10 **Abstract**

11 Dansgaard–Oeschger (D–O) warming events are comparable in magnitude and rate to the
12 anticipated 21st century warming. As such, they provide a good target for evaluation of the
13 ability of state-of-the-art climate models to simulate rapid climate changes. Despite the wealth
14 of qualitative information about climate changes during the D–O events, there has been no
15 attempt to date to make quantitative reconstructions globally. Here we provide reconstructions
16 of seasonal temperature changes and changes in plant-available moisture across multiple D–O
17 events during Marine Isotope Stage 3 based on available pollen records across the globe. These
18 reconstructions show that the largest warming occurred in northern extratropics, especially
19 Eurasia, while western North America and the southern extratropics were characterised by
20 cooling. The change in winter temperature was significantly larger than the change in summer
21 temperature in the northern extratropics, indicating that the D–O warming events were
22 characterised by reduced seasonality, but there is no significant difference between the summer
23 and winter temperature changes in the southern extratropics. The antiphasing between northern
24 and southern extratropical changes, and the west-east pattern of cooling and warming in North
25 America are consistent across the eight D–O events examined, although the signal at individual
26 sites may vary between events. Globally, changes in moisture were positively correlated with
27 changes in temperature, but the strength and the sign of this relationship vary regionally. These
28 reconstructions can be used to evaluate the spatial patterns of changes in temperature and

- 29 moisture in the transient simulations of the D-O events planned as part of the Palaeoclimate
30 Modelling Intercomparison Project.

31 1. Introduction

32 Dansgaard–Oeschger (D–O) events are characterised in Greenland by a transition from cold
33 Greenland Stadial (GS) to warmer Greenland Interstadial (GI) conditions (Dansgaard et al.,
34 1993). The surface air temperature in Greenland increased by 10–15° C during the warming
35 phases; these warming events occur over an interval of between 50 and 200 years (Huber et
36 al., 2006; Kindler et al., 2014). Thus, the D-O events offer a parallel in terms of speed to
37 projected future warming, although both the baseline state and the mechanism inducing this
38 warming differ from anticipated 21st century climate changes. D-O events could therefore
39 provide an opportunity to determine how well climate models that are used for future
40 projections can simulate rapid climate changes (Malmierca-Vallet et al., 2023), particularly
41 regional patterns of warming (and cooling) that are regarded as a challenge for modelling
42 (Doblas-Reyes et al., 2021; Lee et al., 2021) and are highly important in assessing the
43 vulnerability of human societies to future climate changes (IPCC 2022).

44 D-O events are registered globally (Voelker, 2002; Sánchez Goñi and Harrison, 2010; Harrison
45 and Sánchez Goñi, 2010; Sánchez Goñi et al., 2017; Adolphi et al., 2019; Corrick et al., 2020).
46 Shifts in vegetation types between GI and GS states have been interpreted as primarily a
47 temperature signal in the extratropics and a moisture signal in the tropics (Harrison and
48 Sánchez Goñi, 2010). Speleothem records provide a good time-control on the synchronicity of
49 climate changes globally with the D-O events registered in Greenland (Adolphi et al., 2019;
50 Corrick et al., 2020), but the driver of this signal can either be temperature or precipitation
51 depending on the region. There are quantitative climate reconstructions based on terrestrial
52 pollen records from La Grande Pile (Guiot et al., 1993), Lago Grande di Monticchio (Huntley
53 et al., 1999), Padul (Camuera et al., 2022), El Cañizar de Villarquemado (Wei et al., 2021;
54 Camuera et al., 2022) and Lake Ohrid (Sinopoli et al., 2019), marine cores in the western
55 Mediterranean and offshore from Portugal (Sánchez-Goñi et al., 2002), diatom assemblages at
56 Les Echets, France (Ampel et al., 2010), bacterial membrane lipid records from the Eifel region
57 (Zander et al., 2023), isotopic measurements of earthworm calcite from the Rhine Valley
58 (Prud'homme et al., 2022) and clumped isotope measurements on snails in Hungary (Újvári et
59 al., 2021). Aside from the lack of comparable quantitative estimates from outside Europe,
60 differences in the methodology employed and in the specific climate variables reconstructed in
61 each of these studies limits their usefulness for model evaluation. In particular, given that there
62 is still uncertainty as to whether the D-O cycles are characterised by changes in seasonality

63 such that warming events are primarily driven by changes in winter (Flückiger et al., 2008;
64 Zander et al., 2024), in the regional strength of the warming (Harrison and Sánchez Goñi, 2010)
65 and how warming relates to changes in moisture (Wei et al., 2021), there is a need for more
66 systematic reconstruction of seasonal climate changes.

67 In the paper, we provide reconstructions of seasonal temperature changes and changes in plant-
68 available moisture during the intervals corresponding to D-O warming events in Greenland
69 during Marine Isotope Stage 3 based on available pollen records globally. We employ a
70 standard methodology to construct age models for these records, as well as a standard
71 regression-based approach to make the reconstructions. We analyse the regional patterns to
72 identify key targets for model evaluation.

73 **2. Methods**

74 **2.1. Data sources**

75 Modern pollen data were obtained from version 3 of the SPECIAL Modern Pollen Dataset
76 (SMPDSv3). This global dataset contains 26489 samples from 18086 different locations. The
77 dataset was created after removing taxa that are not climatically diagnostic (e.g. obligate
78 aquatics, carnivorous species, cultivated plants). The dataset provides several levels of
79 taxonomic aggregation; here we use the most aggregated level, where woody species were
80 generally combined at genus level and herbaceous species at sub-family or family level unless
81 they were palynologically distinctive, occupied distinctive ecological niches and were
82 sufficiently geographically widespread. This "amalgamated" dataset contains relative
83 abundance information for 1362 taxa. These samples were aggregated by location (which is
84 longitude, latitude and elevation) in order to remove duplicates. Counts for *Quercus*, *Quercus*
85 (deciduous) and *Quercus* (evergreen) were combined because of inconsistent differentiation of
86 *Quercus* pollen in different regional records. Deciduous and evergreen oaks occupy different
87 areas of climate space, particularly in terms of seasonal moisture; specifically, evergreen oaks
88 are typically found in areas characterised by winter rainfall such as the Mediterranean.
89 Nevertheless, since there are other plant taxa that are similarly diagnostic of such regimes, the
90 amalgamation of *Quercus* (deciduous) and *Quercus* (evergreen) should not have a major effect
91 on the robustness of our climate reconstructions. We have tested this assumption by making
92 reconstructions based on all taxa except *Quercus* (Supplementary Materials, Section 4). Taxa
93 that occurred in less than 10 samples in the training dataset were not used to make

94 reconstructions because it is unlikely that the available samples provided a reasonable estimate
95 of the climate space occupied by these rare taxa (Liu et al., 2020). After the location
96 aggregation and the taxa filter, the dataset contains information on 18086 samples with relative
97 abundance information for 607 taxa (Figure 1).

98 We have used a global pollen dataset for calibration of the pollen-climate relationships. The
99 use of a global dataset, rather than region-specific training data, relies on the principle of
100 phylogenetic niche conservatism (Harvey and Pagel, 1991; Qian and Ricklefs 2004; Wang et
101 al., 2025), which states that traits tend to remain constant over time and that the climatic niches
102 of specific genera are also conservative (Harrison et al., 2025). The use of a global dataset for
103 calibration makes it possible to sample a large range of climates, and thus makes it more likely
104 that the reconstructions of glacial climates are realistic and not confined to the limited climate
105 range sampled in any one region (Turner et al., 2020).

106 The SMPDSv3 also provides climatic information at each pollen site, specifically the mean
107 temperature of the coldest month (MTCO), mean temperature of the warmest month (MTWA),
108 and a plant-available moisture (α) calculated as the ratio of actual evapotranspiration to
109 equilibrium evapotranspiration. These bioclimate variables reflect mechanistically distinct
110 controls on plant growth. α is a transformation of the commonly used moisture index MI
111 (Supplementary Materials, Section 2), to emphasize the differences at the dry end of the climate
112 range, which have a more pronounced effect on vegetation distribution than differences at the
113 wet end (Prentice et al., 2017). The climate space occupied by SMPDSv3 (Figure S1) samples
114 a reasonable range of global climate space and therefore should provide robust reconstructions
115 of climate changes under glacial conditions.

116 The fossil pollen data were obtained from the Abrupt Climate Changes and Environmental
117 Responses (ACER) database (Sánchez Goñi et al., 2017), which includes 93 records from the
118 last glacial period (73-15 ka) with sufficient resolution and dating control to detect sub-
119 millennial scale variability. Here we focus on the 73 records covering most of Marine Isotope
120 Stage 3 (50-30 ka); 54 of these records are from terrestrial sites and 19 from marine sites
121 (Figure 1; Table 1). The fossil data were taxonomically harmonised to be consistent with the
122 SMPDSv3.

123 2.2. Climate reconstruction method

124 We used tolerance-weighted Weighted Averaging Partial Least Squares (*fx*TWA-PLS: Liu et
125 al., 2020; Liu et al., 2023) regression to model the relationships between taxon abundances and
126 individual climate variables in the SMPDSv3 modern training dataset and then applied these
127 relationships to reconstruct past climate using the fossil assemblages from the ACER database
128 (Figure 2). *fx*TWA-PLS reduces the tendency of regression methods to compress
129 reconstructions towards the centre of the sampled climate range by applying a sampling
130 frequency correction to reduce the influence of uneven sampling of climate space and
131 weighting the contribution of individual taxa according to their climate tolerances (Liu et al.,
132 2020). Version 2 of *fx*TWA-PLS (*fx*TWA-PLSv2, Liu et al., 2023) uses P-splines smoothing
133 to derive the frequency correction and applies this correction both in estimating the climate
134 optima and tolerances, and in the regression itself, producing a further improvement in model
135 performance compared to *fx*TWA-PLSv1 (Liu et al., 2020).

136 We evaluated the *fx*TWA-PLSv2 models by comparing the reconstructions with observations
137 using leave-out cross-validation, where one site at a time was randomly selected as a test site
138 and sites that are both geographically close (within 50 km horizontal distance from the site)
139 and climatically close (within 2% of the full range of each climate variable in the dataset) were
140 also removed from the training set, to prevent redundancy in the climate information from
141 inflating the cross-validation goodness of fit, following Liu et al. (2020). This ensures that we
142 are not just tuning to the training dataset, and that we can reconstruct climates even when the
143 training set does not completely cover the climate to be reconstructed because there are gaps
144 in the climate space. We selected the last significant number of components (p -value ≤ 0.01)
145 and assessed model performance using the root mean square error of prediction (RMSEP).
146 Compression was assessed using linear regression of the leave-out cross-validated
147 reconstructions on to the climate variable. Reconstructions of MTCO, MTWA and α were
148 made for every sample in each fossil record. Sample specific errors were estimated via
149 bootstrapping, as described in Liu et al. (2020). We corrected for the effect of changes in
150 atmospheric CO₂ on plant water-use efficiency, and hence the reconstructions of α (Figure S2),
151 following Prentice et al. (2022). Appropriate values of CO₂ were taken from the WAIS Divide
152 ice core record (Bauska et al., 2021).

153 2.3. Age modelling

154 Although the ACER database provides age models for each pollen record, the resolution of the
155 individual records is variable (mean resolution 476 years) and these models are often
156 imperfectly aligned with the dating of D-O warming events as recorded in the Greenland ice
157 core, and which have been shown to have a globally synchronous imprint through analysis of
158 speleothem records (Adolphi et al., 2019; Corrick et al., 2020). To create a better alignment,
159 we kept the original age model for marine sites since they are generally calibrated using the
160 oxygen isotope records and are therefore more compatible with the ice core records, and used
161 dynamic time warping (DTW: Belman and Kalaba, 1959; Burstyn et al., 2021; Alshehri et al.,
162 2019) to adjust the age scale for each individual terrestrial record (Figure 2). Dynamic time
163 warping optimises the similarity between two sequences by stretching or compressing one
164 sequence in the time dimension to match the other. Here, we use simulated mean annual
165 temperature (MAT) from a transient simulation of the interval 50-30 ka made with the
166 LOVECLIM model (Menviel et al., 2014) as the reference sequence compared to MAT
167 calculated as the average of MTCO and MTWA from the individual pollen records. We used
168 the mid-point between the start dates of each D-O warming event as recorded in the Greenland
169 ice core (Wolff et al., 2010; converted into AICC2012 timescale) to sub-divide each ACER
170 record into discrete intervals and modified the time scale of the reconstructed mean annual
171 temperature series in each interval to match the reference sequence, having normalised both
172 sequences to remove the influence of differences in absolute values and the amplitude of
173 changes. The adjusted age model for each ACER record was then applied to the reconstructions
174 of MTCO, MTWA, and α from that record for subsequent analyses.

175 2.4. Assessment of regional climate changes during Greenland D-O warming events

176 The magnitude of climate change during the interval corresponding to each D-O warming event
177 as registered in Greenland is calculated individually for each climate variable at each site. To
178 avoid making an assumption about the sign of the climate change at a site, we used a third-
179 order polynomial to fit the reconstructions during the interval from 300 years before to 600
180 years after the official start date corresponding to Greenland D-O warming for each event
181 (Wolff et al., 2010; converted into AICC2012 timescale) to determine whether the change was
182 positive or negative. We then found the ages corresponding to the minimum and maximum in
183 the fitted polynomial ($t_{\min \text{ polynomial}}$, $t_{\max \text{ polynomial}}$). Since the smoothed polynomial may

184 underestimate or overestimate the amplitude of change, we used the reconstructed minimum
 185 or maximum value within the period $t_{\min \text{ polynomial}} \pm 100$ years or $t_{\max \text{ polynomial}} \pm 100$ years
 186 respectively (see Figure S3 for illustration).

187 In cases where no change was registered for all of the three climate variables, we assume that
 188 the event was not registered at the site. As a measure of the accuracy of the DTW method to
 189 identify D-O events, we compared the number of identified events with the number of D-O
 190 events that should occur during the time covered by each record (Table 1). To assess whether
 191 events were missed in a particular record due to low sampling resolution, we examined the
 192 number of samples present in the 900-year interval covering the sampled D-O (i.e. 300 years
 193 before to 600 years after the official start date of each event), where low resolution was defined
 194 as ≤ 3 samples in this 900-year interval. Reconstructions covering intervals where a signal was
 195 not identified were not used in subsequent analyses.

196 We calculated sample-specific errors for the minimum and maximum reconstructed values.
 197 Assuming that the minimum and maximum values are independent, we used error propagation
 198 to obtain the error of the change:

$$199 \quad \sigma_{chan} = \sqrt{\sigma_{min}^2 + \sigma_{max}^2}$$

200 Following Liu et al. (2022), we used a maximum likelihood method to estimate the ratio of
 201 ΔMTCO to ΔMTWA (and ratio of $\Delta\alpha$ to ΔMTWA) to take account of the errors on both
 202 variables.

203 3. Results

204 $f\text{xTWA-PLS}$ reproduces the modern climate reasonably well (Table 2; Figure S4.1 & 4.2). The
 205 performance is best for MTCO ($R^2 = 0.75$, RMSEP = 6.52, slope = 0.85) but is also good for
 206 MTWA ($R^2 = 0.60$, RMSEP = 3.58, slope = 0.72) and α ($R^2 = 0.65$, RMSEP = 0.183, slope =
 207 0.71). Assessment of the variance inflation factor scores shows that there is no problem of
 208 multicollinearity so that it is possible to reconstruct all three climate variables independently
 209 (Supplementary Table 1).

210 The use of dynamic time warping made it possible to identify D-O events robustly (Figure S5.1
 211 ~ S5.8; Table 1; Supplementary Table 2). 13 of the 73 sites cover some part of the 50-30 ka

212 periods but do not include D-O events. Across the remaining 60 sites, we identified 285 out of
213 the 328 individual D-O events (87 %) that should occur during the intervals covered by the
214 records. In the majority of cases where a D-O event should have been registered but could not
215 be identified in an individual record (37 out of 43 cases), the resolution of that part of the record
216 was extremely poor (≤ 3 samples in the 900-year interval starting 300 years before to 600 years
217 after the official start date of the event).

218 ΔMTCO and ΔMTWA were generally largest in the extratropics and were more muted in the
219 tropics (Figure 3). ΔMTCO was found to be significantly larger than ΔMTWA in the northern
220 extratropics when considered across all D-O events and sites; ΔMTCO was found to be larger
221 than ΔMTWA , but not significantly larger, in the southern extratropics; ΔMTCO was found
222 to be not correlated with ΔMTWA in the tropics (Table 3). However, there was a significant
223 positive relationship between the $\Delta\alpha$ and ΔMTWA in all regions (Figure 4; Table 4).

224 The spatial patterns of ΔMTCO and ΔMTWA show consistent features across multiple D-O
225 events (Figure 5), most noticeably that the largest warming occurs in the extratropics of
226 Eurasia, while western North America and the southern extratropics are characterised by
227 cooling. These patterns are also shown if only those reconstructions where the change is twice
228 that of the sample specific error are considered (Figure S6), showing that the spatial patterns
229 are robust to the choice of threshold. The anti-phasing between the northern and southern
230 extratropics is consistent across D-O events. Nevertheless, both the magnitude of the changes
231 and the spatial patterns vary between the D-O events (Figure S7.1; Figure S7.2). $\Delta\alpha$ broadly
232 follows the changes in temperature, with increased α in regions characterised by warming
233 (Figure 5) but show more variability both spatially and between D-O events (Figure S7.3). This
234 is particularly true for Europe, which is characterised by a mixed signal of drying and wetting.

235 **4. Discussions and Conclusions**

236 We have presented a first attempt to map the spatial patterns of quantitative changes in seasonal
237 temperature and plant-available moisture during D-O events globally, using a consistent
238 methodology and a single data source. These analyses show that there is an anti-phasing
239 between changes in the northern extratropics and the southern extratropics, with warming in
240 the north and cooling in the south. The largest and most consistent warming during D-O events
241 occurs in Eurasia. There is a significant difference in the warming during winter and summer
242 in the northern extratropics, resulting in an overall reduction in seasonality, but no significant

243 difference in the southern extratropics. Site-based reconstructions (e.g. Denton et al., 2022;
244 Zander et al., 2024) suggest much larger cooling in winter than summer during cold phases of
245 the last glacial, implying enhanced seasonality compared to warm intervals, which would be
246 consistent with our reconstructions of a reduction in seasonality during warming events in the
247 northern extratropics. Globally, there is a positive relationship between the change in
248 temperature and plant available moisture, as indicated by α . This is consistent with more
249 qualitative interpretation of palaeo-records from specific regions, where many regions are
250 characterised by both warming and wetting (e.g. western Europe: Sánchez Goñi et al., 2008;
251 Fletcher et al., 2010; eastern Europe: Fleitmann et al., 2009; Stockehecke et al., 2016; central
252 Siberia: Grygar et al., 2006; the Great Basin USA: Denniston et al., 2007; Jiménez-Moreno et
253 al., 2010). However, according to our reconstructions, the nature of this relationship varies
254 between regions: there are some regions that are characterised by warming and wetting, others
255 are characterised by warming and drying (Figure 4; Figure 5). Previous studies have also
256 indicated drier conditions during D-O events, particularly in parts of the USA such as the
257 Pacific Northwest (Grigg and Whitlock, 2002) and Florida (Grimm et al., 2006; Jiménez-
258 Moreno et al., 2010). Although there is some consistency in the broadscale patterns of changes
259 across D-O events, the magnitude of the changes as well as the spatial patterning varies
260 between events (Figure S7.1~ 7.3).

261 We have used a global pollen data set for calibration of the pollen-climate relationships. The
262 use of a global data set, rather than region-specific training data, relies on the principle of
263 phylogenetic niche conservatism (Harvey and Pagel, 1991; Qian and Ricklefs 2004; Wang et
264 al., 2025), which states that traits tend to remain constant over time. This also applies to the
265 climate niche (Wiens and Graham, 2005; Wiens et al., 2010; Peterson, 2011; Crisp and Cook,
266 2012; Jiang et al., 2023) as evidenced by disjunct distributions of taxa across different
267 continents (Yin et al., 2021). Niche conservatism underpins the fact that the modern
268 distribution of specific genera can be predicted using climate-pollen relationships developed
269 from other regions (e.g. Huntley et al., 1989). The use of a global dataset for calibration makes
270 it possible to sample a large range of climates, and specifically to reconstruct climate variables
271 that might be very different from the range experienced in a region in the modern day. This is
272 particularly important when reconstructing changes in the fundamentally different climate of
273 the last glacial. Reconstructed glacial climates at some sites were indeed found to exceed the
274 climate ranges sampled for the region under modern conditions, most noticeably MTCO and
275 MTWA in the southern extratropics (Figure S8). However, the use of a global data set can

276 create issues because of inconsistencies in taxonomic resolution between regions. The
277 necessity for treating all species of *Quercus* as a single taxon, despite the fact that evergreen
278 and deciduous species may occupy distinct climate niches in some regions such as Europe, is
279 a consequence of this. However, we have shown (Supplementary Materials, Section 4) that this
280 has little impact on our reconstructions – largely because the climatic distinction that would be
281 conveyed through separating deciduous and evergreen *Quercus* is also registered by the
282 presence of other taxa. Although the use of a global training data set for climate reconstructions
283 has not been a common practice, it also facilitates making reconstructions for sites from regions
284 with limited modern pollen data or where the modern samples do not capture the very different
285 climates that might have occurred in that region during glacial times.

286 These reconstructions can be used as targets for model evaluation, specifically the two transient
287 D-O experiments planned for the next phase of the Palaeoclimate Modelling Intercomparison
288 (see Malmierca-Vallet et al., 2023 for the experimental protocol). The first of these experiments
289 is a baseline simulation starting at 34 ka, a time with low obliquity, moderate MIS3 greenhouse
290 gas values, and an intermediate ice sheet configuration, which appears to be most conducive to
291 generating D-O like behaviour in climate models. The second experiment involves the addition
292 of freshwater, to examine whether this is necessary to precondition a state conducive to
293 generating D-O events. The observed anti-phasing in temperature changes between the
294 northern and southern hemispheres is a general feature of climate model experiments. Most
295 models show larger warming in winter than in summer in the northern hemisphere (e.g.
296 Flückiger et al., 2008; Van Meerbeeck et al., 2011; Izumi et al., 2023), which is also consistent
297 with our reconstructions. Models generally show an intensification of the northern hemisphere
298 monsoons during D-O events (e.g. Menviel et al., 2020; Izumi et al., 2023), but there is less
299 consistency about changes in plant-available moisture in the extratropics. Our reconstructions
300 of α suggest an intensification of the northern hemisphere monsoons, consistent with the
301 simulations, and provide an opportunity to evaluate spatial patterns of moisture changes over
302 the extratropics. The reconstructions also indicate an increase in α across much of the tropics,
303 including northern South America, southern China and Japan (Figure 5). Although α is not a
304 direct reflection of summer precipitation, these changes are consistent with enhanced northern
305 hemisphere monsoons during warming events, as shown by speleothem records from the
306 Caribbean (Warren et al., 2019) and speleothem and pollen records from Asia (Wang et al.,
307 2001; Zorzi et al., 2022; Fohlmeister et al., 2023).

308 The LOVECLIM model is used as a reference to adjust the age scale in the reconstructions
309 using MAT, but this does not preclude comparison of the reconstructed and simulated seasonal
310 temperatures. The general spatial pattern of simulated changes in MTCO and MTWA (Figure
311 S9.1) is consistent with the reconstructions, with largest warming in Eurasia, and cooling over
312 most of the southern extratropical land. However, there are important differences. The
313 reconstructions show cooling over western North America in both seasons, for example, but
314 only in winter in the simulations. The relationship between ΔMTCO versus ΔMTWA is also
315 different (Figure S9.2): the simulated ΔMTCO is shown to be significantly larger than ΔMTWA
316 in the northern extratropics, but significantly smaller than ΔMTWA in the southern extratropics
317 (Supplementary Table 3). This comparison illustrates the usefulness of the reconstructions for
318 model evaluation and to investigate the mechanisms that may not be adequately captured by
319 current models.

320 Identifying D-O events in pollen records is often problematic, particularly in regions where
321 warming (especially if accompanied by dryer conditions) leads to a reduction (or an hiatus) in
322 sedimentation as reflected in the variable resolution of the available pollen records (e.g.
323 Sinopoli et al., 2019; Wei et al., 2021; Camuera et al., 2022; Pini et al., 2022). The use of
324 dynamic time warping (DTW: Belman and Kalaba, 1959; Burstyn et al., 2021; Alshehri et al.,
325 2019) goes some way to improving the identification of potential D-O events. However, it
326 precludes the calculation of a rate of change in climate. Thus, we have focused here on the
327 absolute magnitude of the changes during specific warming events. It is also likely that some
328 of the variability in the reconstructed changes between different D-O events reflects imperfect
329 identification of specific events because of the comparatively modest resolution of the records.
330 Several new high-resolution records covering MIS3 have become available since the
331 compilation of the ACER database (e.g. Bird et al., 2024; Wei et al., 2021; Camuera et al.,
332 2022; Pini et al., 2022; Rowe et al., 2024; Shichi et al., 2023; Zorzi et al., 2022) and including
333 these newer records could help to improve the reliability of the global reconstructions presented
334 here.

335

336 **Data and code availability.** All the data used are public access and cited here. The code used
337 to generate the reconstructions and figures is available at [https://github.com/ml4418/DO-](https://github.com/ml4418/DO-climate-reconstruction-paper.git)
338 [climate-reconstruction-paper.git](https://github.com/ml4418/DO-climate-reconstruction-paper.git)

339 **Author contributions.** ML, SPH and ICP designed the study. ML made the reconstructions
340 and produced the figures and tables. ML and SPH carried out the analyses. SPH wrote the first
341 draft of the paper and all authors contributed to the final draft.

342 **Competing Interests.** The authors declare not competing interests.

343 **Acknowledgements.** ML acknowledges support from Imperial College through the Lee
344 Family Scholarship. ICP acknowledges support from the ERC under the European Union
345 Horizon 2020 research and innovation programme (grant agreement no.: 787203 REALM).
346 SPH acknowledges fruitful discussions with colleagues from the D-O community working
347 group.

348

349 **References**

350 Adolphi, F., Bronk Ramsey, C., Erhardt, T., Edwards, R. L., Cheng, H., Turney, C. S. M.,
351 Cooper, A., Svensson, A., Rasmussen, S. O., Fischer, H., and Muscheler, R.:
352 Connecting the Greenland ice-core and U/Th timescales via cosmogenic radionuclides:
353 testing the synchronicity of Dansgaard–Oeschger events, *Clim. Past*, 14, 1755–1781,
354 <https://doi.org/10.5194/cp-14-1755-2018>, 2018.

355 Alshehri, M., Coenen, F., and Dures, K.: Effective sub-sequence-based dynamic time warping.
356 In: Bramer, M., Petridis, M. (eds) *Artificial Intelligence XXXVI. SGAI 2019. Lecture*
357 *Notes in Computer Science*, 11927. Springer, Cham. [https://doi.org/10.1007/978-3-](https://doi.org/10.1007/978-3-030-34885-4_23)
358 [030-34885-4_23](https://doi.org/10.1007/978-3-030-34885-4_23), 2019.

359 Ampel, L., Bigler, C., Wohlfarth, B., Risberg, J., Lotter, A.F., and Veres, D.: Modest summer
360 temperature variability during DO cycles in western Europe, *Quat. Sci. Rev.*, 29, 1322–
361 1327, <https://doi.org/10.1016/j.quascirev.2010.03.002>, 2010.

362 Bauska, T. K., Marcott, S. A. and Brook, E. J.: Abrupt changes in the global carbon cycle
363 during the last glacial period, *Nat. Geosci.*, 14(2), 91–96, doi:10.1038/s41561-020-
364 00680-2, 2021.

- 365 Bellman, R., and Kalaba, R.: On adaptive control processes, *Automatic Control, IRE*
366 *Transactions*, 4, 1–9, http://ieeexplore.ieee.org/xpls/abs_all.jsp?arnumber=1104847,
367 1959.
- 368 Bird, M., Brand, M., Comley, R., Fu, X., Hadeen, X., Jacobs, Z., Rowe, C., Wurster, C., Zwart,
369 C. and Bradshaw, C.: Late Pleistocene emergence of an anthropogenic fire regime in
370 Australia's tropical savannahs, *Nat. Geosci.*, 17, doi:10.1038/s41561-024-01388-3,
371 2024.
- 372 Burstyn, Y., Gazit, A., and Omri Dvir, O.: Hierarchical Dynamic Time Warping methodology
373 for aggregating multiple geological time series, *Comp. & Geosci.*, 150, 104704,
374 <https://doi.org/10.1016/j.cageo.2021.104704>, 2021.
- 375 Camuera, J., Ramos-Román, M.J., Jiménez-Moreno, G. *et al.*: Past 200 kyr hydroclimate
376 variability in the western Mediterranean and its connection to the African Humid
377 Periods, *Sci. Rep.*, 12, 9050, <https://doi.org/10.1038/s41598-022-12047-1>, 2022.
- 378 Corrick, E.C., Drysdale, R.N., Hellstrom, J.C., Capron, E., Rasmussen, S.O., Zhang, X.,
379 Fleitmann, D., Couchoud, I., and Wolff, E.: Synchronous timing of abrupt climate
380 changes during the last glacial period, *Science*, 369, 963–969,
381 <https://doi.org/10.1126/science.aay5538>, 2020.
- 382 Crisp, M. D. and Cook, L. G.: Phylogenetic niche conservatism: What are the underlying
383 evolutionary and ecological causes?, *New Phytol.*, 196(3), 681–694,
384 doi:10.1111/j.1469-8137.2012.04298.x, 2012.
- 385 Dansgaard, W., Johnsen, S.J., Clausen, H.B., Dahl-Jensen, D., Gundestrup, N.S., Hammer,
386 C.U., Hvidberg, C.S., Steffensen, J.P., Sveinbjörnsdóttir, A.E., Jouzel, J., and Bond,
387 G.: Evidence for general instability of past climate from a 250-kyr ice-core record,
388 *Nature*, 364, 218–220, <https://doi.org/10.1038/364218a0>, 1993.
- 389 Denniston, R.F., Asmerom, Y., Polyak, V., Dorale, J.A., Carpenter, S.J., Trodick, C., Hoyer,
390 B., and González, L.A.: Synchronous millennial-scale climatic changes in the Great
391 Basin and the North Atlantic during the last interglacial. *Geology* 35, 619–622, 2007.
- 392 Doblus-Reyes, F. J., Sörensson, A. A., Almazroui, M., Dosio, A., Gutowski, W. J., Haarsma,
393 R., Hamdi, R., Hewitson, B., Kwon, W.-T., Lamptey, B. L., Maraun, D., Stephenson,

- 394 T. S., Takayabu, I., Terray, L., Turner, A. and Zuo, Z.: Linking global to regional
395 climate change, in *Climate Change 2021 – The Physical Science Basis: Working Group*
396 *I Contribution to the Sixth Assessment Report of the Intergovernmental Panel on*
397 *Climate Change*, edited by V. Masson-Delmotte, P.Zhai, A. Pirani, S. L. Connors, C.
398 Péan, S. Berger, N. Caud, Y. Chen, L. Goldfarb, M. I. Gomis, M. Huang, K. Leitzell,
399 E.Lonnoy, J. B. R. Matthews, T. K. Maycock, T. Waterfield, O. Yelekçi, R. Yu, and B.
400 Zhou, pp. 1363–1512, Cambridge University Press, Cambridge, United Kingdom and
401 New York, NY, USA., 2021.Fleitmann, D., Cheng, H., Badertscher, S., Edwards, R.L.,
402 Mudelsee, M., Gökürk, O.M., Fankhauser, A., Pickering, R., Raible, C.C., Matter, A.,
403 Kramers, J., and Tüysüz, O.: Timing and climatic impact of Greenland interstadials
404 recorded in stalagmites from northern Turkey, *Geophys. Res. Lett.*, 36, 2009.
- 405 Fletcher, W.F., Sánchez Goñi, M.F., Allen, J.R.M., Cheddadi, R., Combourieu-Nebout, N.,
406 Huntley, B., Lawson, I., Londeix, L., Magri, D., Margari, V., Müller, U.C., Naughton,
407 F., Novenko, E., Roucoux, K., Tzedakis, P.C.: Millennial-scale variability during the
408 last glacial in vegetation records from Europe, *Quat. Sci. Rev.*, 29, 2839-2864,
409 <https://doi.org/10.1016/j.quascirev.2009.11.015>, 2010.
- 410 Flückiger, J., Knutti, R., White, J.W.C., and Renssen, H.: Modeled seasonality of glacial abrupt
411 climate events, *Clim. Dyn.*, 31, 633–645, <https://doi.org/10.1007/s00382-008-0373-y>,
412 2008.
- 413 Fohlmeister, J., Sekhon, N., Columbu, A., Vettoretti, G., Weitzel, N., Rehfeld, K., Veiga-Pires,
414 C., Ben-Yami, M., Marwan, N. and Boers, N.: Global reorganization of atmospheric
415 circulation during Dansgaard–Oeschger cycles, *Proc. Natl. Acad. Sci.*, 120(36),
416 e2302283120, doi:10.1073/pnas.2302283120, 2023.
- 417 Grigg, L.D., and Whitlock, C.: Patterns and causes of millennial-scale climate change in the
418 Pacific Northwest during Marine Isotope Stages 2 and 3, *Quat. Sci. Rev.*, 21, 2067-
419 2083, 2002.
- 420 Grimm, E.C., Watts, W.A., Jacobson, G.L., Hansen, B.C.S., Almquist, H., and Dieffenbacher-
421 Krall, A.C.: Evidence for warm wet Heinrich events in Florida, *Quat. Sci. Rev.*, 25,
422 2197-2211, 2006.

- 423 Grygar, T., Kadlec, J., Pruner, P., Swann, G., Bezdicka, P., Hradil, D., Lang, K., Novotna, K.,
424 and Oberhänsli, H.: Paleoenvironmental record in Lake Baikal sediments:
425 environmental changes in the last 160 ky, *Palaeogeogr. Palaeoclimatol. Palaeoecol.*,
426 237, 240-254, 2006.
- 427 Guiot, J., de Beaulieu, J. L., Cheddadi, R., David, F., Ponel, P., and Reille, M.: The climate in
428 Western Europe during the last Glacial/Interglacial cycle derived from pollen and insect
429 remains, *Palaeogeogr., Palaeoclimatol., Palaeoecol.*, 103, 73–93,
430 [https://doi.org/10.1016/0031-0182\(93\)90053-L](https://doi.org/10.1016/0031-0182(93)90053-L), 1993.
- 431 Jiménez-Moreno, G., Anderson, R.S., Desprat, S., Grigg, L.D., Grimm, E.C., Heusser, L.E.,
432 Jacobs, B.F., López-Martínez, C., Whitlock, C.L., and Willard, D.A.: Millennial-scale
433 variability during the last glacial in vegetation records from North America, *Quat. Sci.*
434 *Rev.*, 29, 2865-2881, <https://doi.org/10.1016/j.quascirev.2009.12.013>, 2010.
- 435 Harrison, S.P., and Sánchez Goñi, M.F.: Global patterns of vegetation response to millennial-
436 scale variability during the last glacial: A synthesis. *Quat. Sci. Rev.*, 29, 2957-2980,
437 2010.
- 438 Harrison, S.P., Bartlein, P.J., Cruz-Silva, E., Haas, O., Jackson, S.T., Kaushal, N., Liu, M.,
439 Magri, D., Robson, D., Vettoretti, G., Prentice, I.C.: Palaeoclimate perspectives on
440 contemporary climate change, *Ann. Rev. Environ. Resour.*, 50, 2025.
- 441 Harvey, P. H. and Pagel, M. D.: *The comparative method in evolutionary biology*, Oxford
442 University Press., 1991.
- 443 Huber, C., Leuenberger, M., Spahni, R., Flückiger, J., Schwander, J., Stocker, T.F., Johnsen,
444 S., Landais, A., and Jouzel, J.: Isotope calibrated Greenland temperature record over
445 Marine Isotope Stage 3 and its relation to CH₄, *Earth Planet. Sci. Lett.*, 243, 504–519,
446 2006.
- 447 Huntley, B., Bartlein, P. J. and Prentice, I. C.: Climatic control of the distribution and
448 abundance of Beech (*Fagus L.*) in Europe and North America, *J. Biogeogr.*, 16(6), 551–
449 560, [doi:10.2307/2845210](https://doi.org/10.2307/2845210), 1989.
- 450 Huntley, B., Watts, W.A., Allen, J.R.M., Zolitschka, B.: Palaeoclimate, chronology and
451 vegetation history of the Weichselian Lateglacial: comparative analysis of data from

- 452 three cores at Lago Grande di Monticchio, southern Italy, *Quat. Sci. Rev.*,18: 945-960,
453 [https://doi.org/10.1016/S0277-3791\(99\)00007-4](https://doi.org/10.1016/S0277-3791(99)00007-4), 1999.
- 454 IPCC: *Climate change 2022: Impacts, adaptation and vulnerability. Contribution of working*
455 *group II to the sixth assessment report of the Intergovernmental Panel on Climate*
456 *Change*, edited by H.-O. Pörtner, D. C. Roberts, M. Tignor, E. S. Poloczanska, K.
457 Mintenbeck, A. Alegría, M. Craig, S. Langsdorf, S. Löschke, V. Möller, A. Okem, and
458 B. Rama, Cambridge University Press, Cambridge University Press, Cambridge, UK
459 and New York, NY, USA., 2022.
- 460 Jiang, K., Wang, Q., Dimitrov, D., Luo, A., Xu, X., Su, X., Liu, Y., Li, Y., Li, Y. and Wang, Z.:
461 Evolutionary history and global angiosperm species richness–climate relationships,
462 *Glob. Ecol. Biogeogr.*, 32(7), 1059–1072, doi:10.1111/geb.13687, 2023.
- 463 Kindler, P., Guillevic, M., Baumgartner, M., Schwander, J., Landais, A., and Leuenberger, M.:
464 Temperature reconstruction from 10 to 120 kyr b2k from the NGRIP ice core, *Clim.*
465 *Past*, 10, 887–902, <https://doi.org/10.5194/cp-10-887-2014>, 2014.
- 466 Lee, J.-Y., Marotzke, J., Bala, G., Cao, L., Corti, S., Dunne, J. P., Engelbrecht, F., Fischer, E.,
467 Fyfe, J. C., Jones, C., Maycock, A., Mutemi, J., Ndiaye, O., Panickal, S. and Zhou, T.:
468 Future global climate: Scenario-based projections and near- term information, in
469 *Climate change 2021: The physical science basis. Contribution of working group I to*
470 *the sixth assessment report of the Intergovernmental Panel on Climate Change*, edited
471 by V. Masson-Delmotte, P. Zhai, A. Pirani, S. L. Connors, C. Péan, S. Berger, N. Caud,
472 Y. Chen, L. Goldfarb, M. I. Gomis, M. Huang, K. Leitzell, E. Lonnoy, J. B. R.
473 Matthews, T. K. Maycock, T. Waterfield, O. Yelekçi, R. Yu, and B. Zhou, pp. 553–672,
474 Cambridge University Press, Cambridge, United Kingdom and New York, NY, USA.,
475 2021.
- 476 Liu, M., Prentice, I.C., ter Braak, C.J.F, and Harrison, S.P.: An improved statistical approach
477 for reconstructing past climates from biotic assemblages, *Proc. Royal Soc., Math. A*,
478 476, 20200346, 20200346, <https://doi.org/10.1098/rspa.2020.0346>, 2020.
- 479 Liu, M., Shen, Y., González-Sampériz, P., Gil-Romera, G., ter Braak, C.J.F. Prentice, I.C., and
480 Harrison, S.P.: Holocene climates of the Iberian Peninsula, *Clim. Past* 19, 803-834,
481 <https://doi.org/10.5194/cp-19-803-2023>, 2023.

- 482 Malmierca-Vallet, I., Sime, L.C., and the D–O community members: Dansgaard–Oeschger
483 events in climate models: review and baseline Marine Isotope Stage 3 (MIS3) protocol,
484 *Clim. Past*, 19, 915–942, <https://doi.org/10.5194/cp-19-915-2023>, 2023.
- 485 Menviel, L., Timmermann, A., Friedrich, T., and England, M. H.: Hindcasting the continuum
486 of Dansgaard–Oeschger variability: mechanisms, patterns and timing, *Clim. Past* 10,
487 63–77, 2014.
- 488 Menviel, L.C., Skinner, L.C., Tarasov, L., and Tzedakis, P.C.: An ice–climate oscillatory
489 framework for Dansgaard–Oeschger cycles, *Nat. Rev. Earth Environ.*, 1, 677–693,
490 <https://doi.org/10.1038/s43017-020-00106-y>, 2020.
- 491 Peterson, A. T.: Ecological niche conservatism: A time-structured review of evidence, *J.*
492 *Biogeogr.*, 38(5), 817–827, doi:10.1111/j.1365-2699.2010.02456.x, 2011.
- 493 Pini, R., Furlanetto, G., Vallé, F., Badino, F., Wick, L., Anselmetti, F.S., Bertuletti, P., Fusi, N.,
494 Morlock, M.A., Delmonte, B., Harrison, S.P., Maggi, V., Ravazzi, C.: Linking North
495 Atlantic and Alpine Last Glacial Maximum climates via a high-resolution pollen-based
496 subarctic forest steppe record, *Quat. Sci. Rev.*, 294, 107759,
497 <https://doi.org/10.1016/j.quascirev.2022.107759>, 2022.
- 498 Prentice, I. C., Cleator, S. F., Huang, Y. H., Harrison, S. P. and Roulstone, I.: Reconstructing
499 ice-age palaeoclimates: Quantifying low-CO₂ effects on plants, *Glob. Planet. Change*,
500 149, 166–176, doi:<https://doi.org/10.1016/j.gloplacha.2016.12.012>, 2017.
- 501 Prentice, I. C., Villegas-Diaz, R. and Harrison, S. P.: Accounting for atmospheric carbon
502 dioxide variations in pollen-based reconstruction of past hydroclimates, *Glob. Planet.*
503 *Change*, 211, 103790, doi:10.1016/j.gloplacha.2022.103790, 2022.
- 504 Prud'homme, C., Fischer, P., Jöris, O., Gromov, S., Vinnepand, M., Hatté, C., Vonhof, H.,
505 Moine, O., Vött, A., and Fitzsimmons, K. E.: Millennial-timescale quantitative
506 estimates of climate dynamics in central Europe from earthworm calcite granules in
507 loess deposits, *Commun. Earth Environ.*, 3, 1–14, [https://doi.org/10.1038/s43247-022-](https://doi.org/10.1038/s43247-022-00595-3)
508 00595-3, 2022.

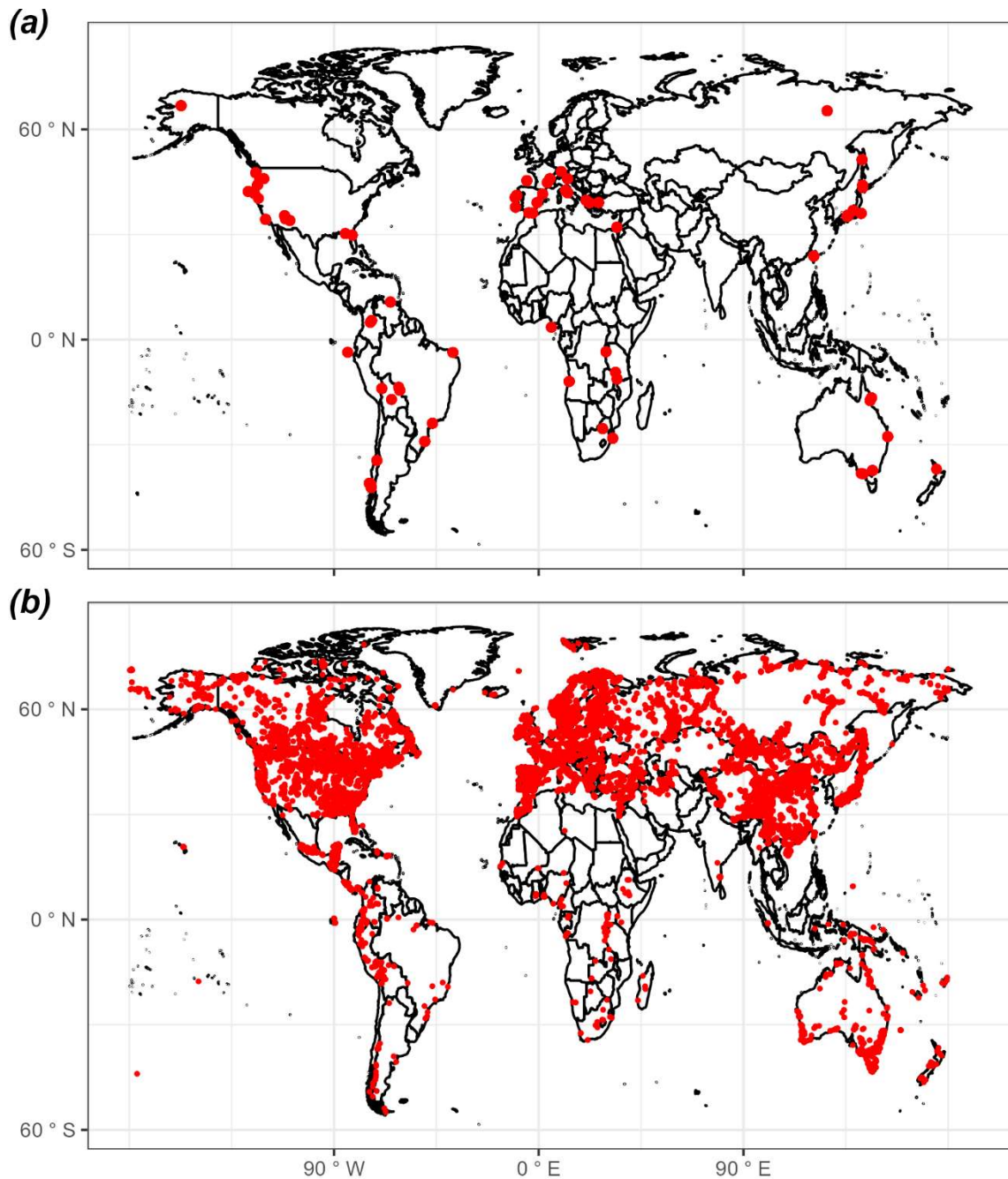
- 509 Qian, H. and Ricklefs, R. E.: Geographical distribution and ecological conservatism of disjunct
510 genera of vascular plants in eastern Asia and eastern North America, *J. Ecol.*, 92(2),
511 253–265, doi:<https://doi.org/10.1111/j.0022-0477.2004.00868.x>, 2004.
- 512 Rowe, C., Brand, M., Wurster, C. M. and Bird, M. I.: Vegetation changes through stadial and
513 interstadial stages of MIS 4 and MIS 3 based on a palynological analysis of the
514 Girraween Lagoon sediments of Darwin, Australia, *Palaeogeogr. Palaeoclimatol.*
515 *Palaeoecol.*, 642, 112150, doi:[10.1016/j.palaeo.2024.112150](https://doi.org/10.1016/j.palaeo.2024.112150), 2024.
- 516 Sánchez Goñi, M., Cacho, I., Turon, J., Guiot, J., Sierro, F., Peyrouquet, J., Grimalt, J. and
517 Shackleton, N.: Synchronicity between marine and terrestrial responses to millennial
518 scale climatic variability during the last glacial period in the Mediterranean region,
519 *Clim. Dyn.*, 19(1), 95–105, doi:[10.1007/s00382-001-0212-x](https://doi.org/10.1007/s00382-001-0212-x), 2002.
- 520 Sánchez Goñi, M.F., and Harrison, S.P.: Millennial-scale climate variability and vegetation
521 changes during the Last Glacial: Concepts and terminology, *Quat. Sci. Rev.*, 29, 2823–
522 2827, 2010.
- 523 Sánchez Goñi, M.F., Desprat, S., Daniau, A.-L., Bassinot, F., Polanco-Martínez, J.M., Harrison,
524 S.P., Allen, J.R.P., Anderson, R.S., Behling, H., Bonnefille, R., Burjachs, F., Carrión,
525 J.S., Cheddadi, R., Clark, J.S., Combourieu-Nebout, N., Courtney-Mustaphi, C.,
526 Debusk, G.H., Dupont, L.M., Finch, J., Fletcher, W.J., Giardini, M., González, C.,
527 Gosling, W.D., Grigg, L.D., Grimm, E.C., Hayashi, R., Helmens, K., Heusser, L.E.,
528 Hill, T., Hope, G., Huntley, B., Igarashi, Y., Irino, T., Jacobs, B.F., Jiménez-Moreno, G.,
529 Kawai, S., Kershaw, P., Kumon, F., Lawson, I., Ledru, M.-P., Lézine, A.-M., Liew, P.-
530 M., Magri, D., Marchant, R., Margari, V., Mayle, F., McKenzie, M., Moss, P., Müller,
531 S., Müller, U.C., Naughton, F., Newnham, R.M., Oba, T., Pérez-Obiol, R., Pini, R.,
532 Ravazzi, C., Roucoux, K.H., Rucina, S., Scott, L., Takahara, H., Tzedakis, P.C., Urrego,
533 D.H., Van Geel, B., Valencia, B.G., Vandergoes, M.J., Vincens, A., Whitlock, C.L.,
534 Willard, D. A., and Yamamoto, M.: The ACER pollen and charcoal database: a global
535 resource to document vegetation and fire response to abrupt climate changes of the last
536 glacial period, *Earth Syst. Sci. Data* 9: 679-695, 2017.
- 537 Shichi, K., Goebel, T., Izuho, M. and Kashiwaya, K.: Climate amelioration, abrupt vegetation
538 recovery, and the dispersal of *Homo sapiens* in Baikal Siberia, *Sci. Adv.*, 9(38),
539 eadi0189, doi:[10.1126/sciadv.adi0189](https://doi.org/10.1126/sciadv.adi0189), 2024.

- 540 Sinopoli, G., Peyron, O., Masi, A., Holtvoeth, J., Francke, A., Wagner, B., and Sadori, L.:
541 Pollen-based temperature and precipitation changes in the Ohrid Basin (western
542 Balkans) between 160 and 70 ka, *Clim. Past*, 15, 53–71, [https://doi.org/10.5194/cp-15-](https://doi.org/10.5194/cp-15-53-2019)
543 53-2019, 2019.
- 544 Stockhecke, M., Timmermann, A., Kipfer, R., Haug, G.H., Kwiecien, O., Friedrich, T.,
545 Menviel, L., Litt, T., Pickarski, N., and Anselmetti, F.S.: Millennial to orbital-scale
546 variations of drought intensity in the Eastern Mediterranean, *Quat. Sci. Rev.*, 133, 77-
547 95, 2016.
- 548 Turner, M. G., Wei, D., Prentice, I. C. and Harrison, S. P.: The impact of methodological
549 decisions on climate reconstructions using WA-PLS, *Quat. Res.*, 99, 341–356,
550 [doi:10.1017/qua.2020.44](https://doi.org/10.1017/qua.2020.44), 2021.
- 551 Újvári, G., Bernasconi, S. M., Stevens, T., Kele, S., Páll-Gergely, B., Surányi, G., and Demény,
552 A.: Stadial-interstadial temperature and aridity variations in east central Europe
553 preceding the Last Glacial Maximum, *Paleoceanog. Paleoclim.*, 36, e2020PA004170,
554 <https://doi.org/10.1029/2020PA004170>, 2021.
- 555 Van Meerbeeck, C.J., Renssen, H., Roche, D.M., Wohlfarth, B., Bohncke, S.J.P., Bos, J.A.A.,
556 Engels, S., Helmens, K.F., Sánchez-Goñi, M.F., Svensson, A., and Vandenberghe, J.:
557 The nature of MIS 3 stadial-interstadial transitions in Europe: New insights from
558 model-data comparisons, *Quat. Sci. Rev.*, 30, 3618–3637,
559 <https://doi.org/10.1016/j.quascirev.2011.08.002>, 2011.
- 560 Voelker, A.H.: Global distribution of centennial-scale records for Marine Isotope Stage (MIS)
561 3: a database, *Quat. Sci. Rev.*, 21, 1185–1212, 2002.
- 562 Wang, Y. J., Cheng, H., Edwards, R. L., An, Z. S., Wu, J. Y., Shen, C.-C. and Dorale, J. A.: A
563 high-resolution absolute-dated Late Pleistocene monsoon record from Hulu Cave,
564 China, *Science (80-.)*, 294(5550), 2345–2348, [doi:10.1126/science.1064618](https://doi.org/10.1126/science.1064618), 2001.
- 565 Wang, C., Wang, M., Zhu, S., Wu, X., Yang, S., Yan, Y. and Wen, Y.: Multiple ecological
566 niche modeling reveals niche conservatism and divergence in East Asian Yew (*Taxus*),
567 *Plants*, 14(7), [doi:10.3390/plants14071094](https://doi.org/10.3390/plants14071094), 2025.

- 568 Warken, S. F., Scholz, D., Spötl, C., Jochum, K. P., Pajón, J. M., Bahr, A. and Mangini, A.:
569 Caribbean hydroclimate and vegetation history across the last glacial period, *Quat. Sci.*
570 *Rev.*, 218, 75–90, doi:10.1016/j.quascirev.2019.06.019, 2019.
- 571 Wei, D., González-Sampériz, P., Gil-Romera, G., Harrison, S.P., and Prentice, I.C.: Seasonal
572 temperature and moisture changes in interior semi-arid Spain from the last interglacial
573 to the Late Holocene, *Quat. Res.*, 101, 143–155, <https://doi.org/10.1017/qua.2020.108>,
574 2021.
- 575 Wiens, J. and Graham, C.: Niche conservatism: Integrating evolution, ecology, and
576 conservation biology, *Annu. Rev. Ecol. Evol. Syst.*, 36, 519–539,
577 doi:10.1146/annurev.ecolsys.36.102803.095431, 2005.
- 578 Wolff, E. W., Chappellaz, J., Blunier, T., Rasmussen, S. O. and Svensson, A.: Millennial-scale
579 variability during the last glacial: The ice core record, *Quat. Sci. Rev.*, 29(21), 2828–
580 2838, doi:10.1016/j.quascirev.2009.10.013, 2010.
- 581 Yin, X., Jarvie, S., Guo, W.-Y., Deng, T., Mao, L., Zhang, M., Chu, C., Qian, H., Svenning, J.-
582 C. and He, F.: Niche overlap and divergence times support niche conservatism in
583 eastern Asia–eastern North America disjunct plants, *Glob. Ecol. Biogeogr.*, 30(10),
584 1990–2003, doi:10.1111/geb.13360, 2021.
- 585 Zander, P. D., Böhl, D., Sirocko, F., Auderset, A., Haug, G. H. and Martínez-García, A.:
586 Reconstruction of warm-season temperatures in central Europe during the past 60 000
587 years from lacustrine branched glycerol dialkyl glycerol tetraethers (brGDGTs), *Clim.*
588 *Past*, 20(4), 841–864, doi:10.5194/cp-20-841-2024, 2024.
- 589 Zorzi, C., Desprat, S., Clément, C., Thirumalai, K., Oliviera, D., Anupama, K., Prasad, S. and
590 Martinez, P.: When eastern India oscillated between desert versus savannah-dominated
591 vegetation, *Geophys. Res. Lett.*, 49(16), e2022GL099417,
592 doi:10.1029/2022GL099417, 2022.
- 593

594 **Figures and Tables**

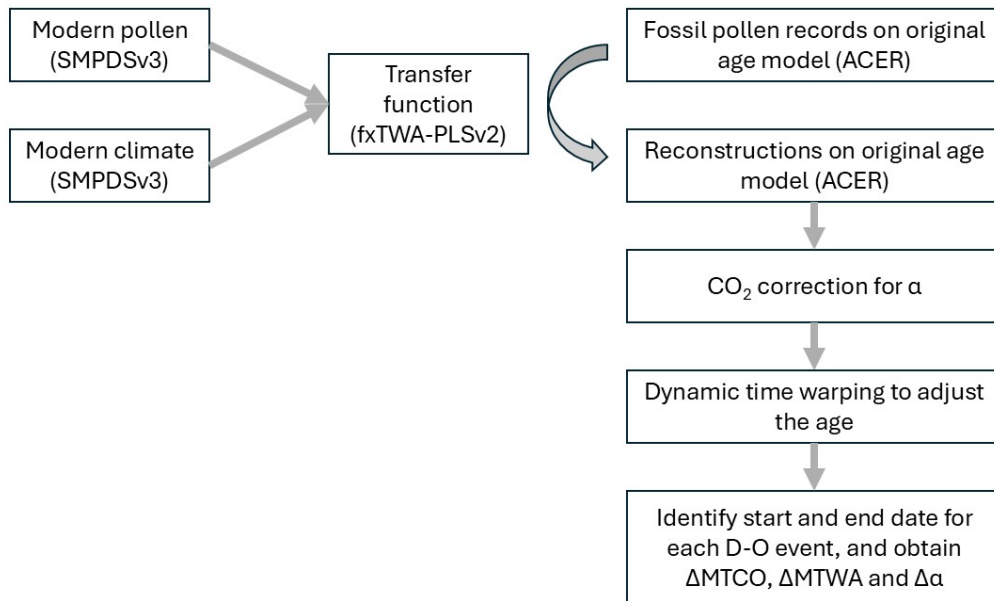
595 Figure 1: Map showing the locations of sites (a) from the Abrupt Climate Changes and
596 Environmental Responses (ACER) database covering the interval between 50 ka and 30 ka
597 used for the reconstructions and (b) sites in version 3 of the SPECIAL Modern Pollen Dataset
598 (SMPDSv3) used to derive the transfer functions for these climate reconstructions.



599

600

601 Figure 2: Flow chart showing the reconstruction methodology.



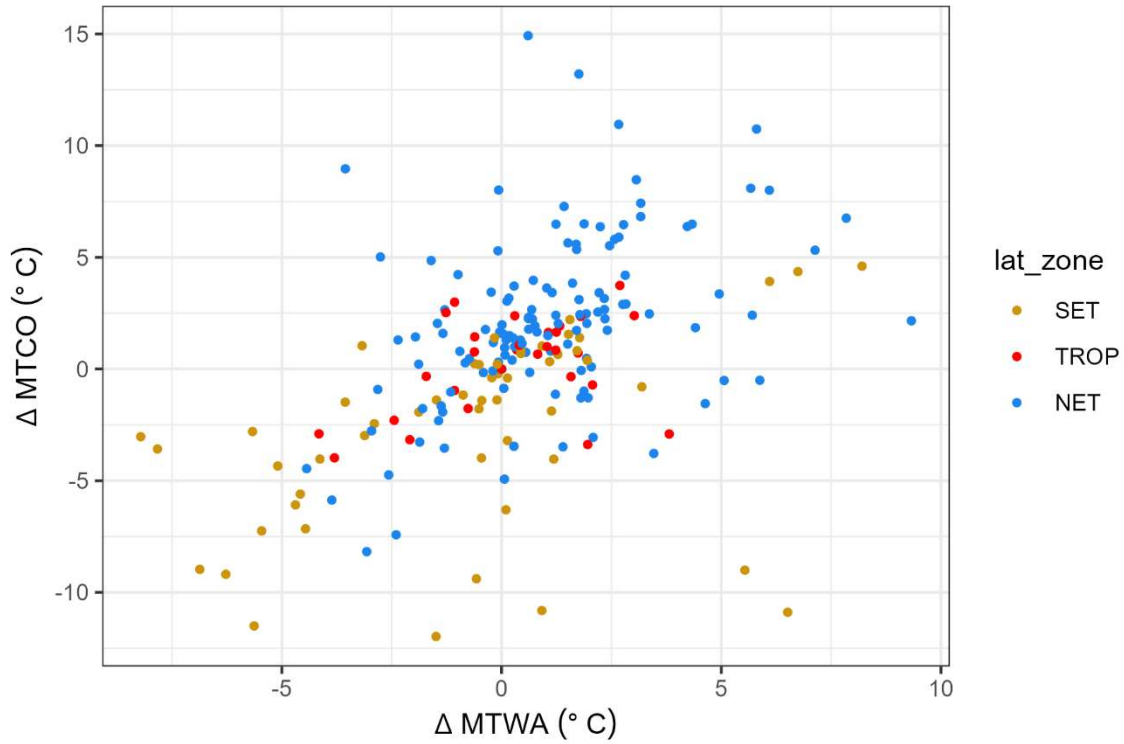
602

603

604

605

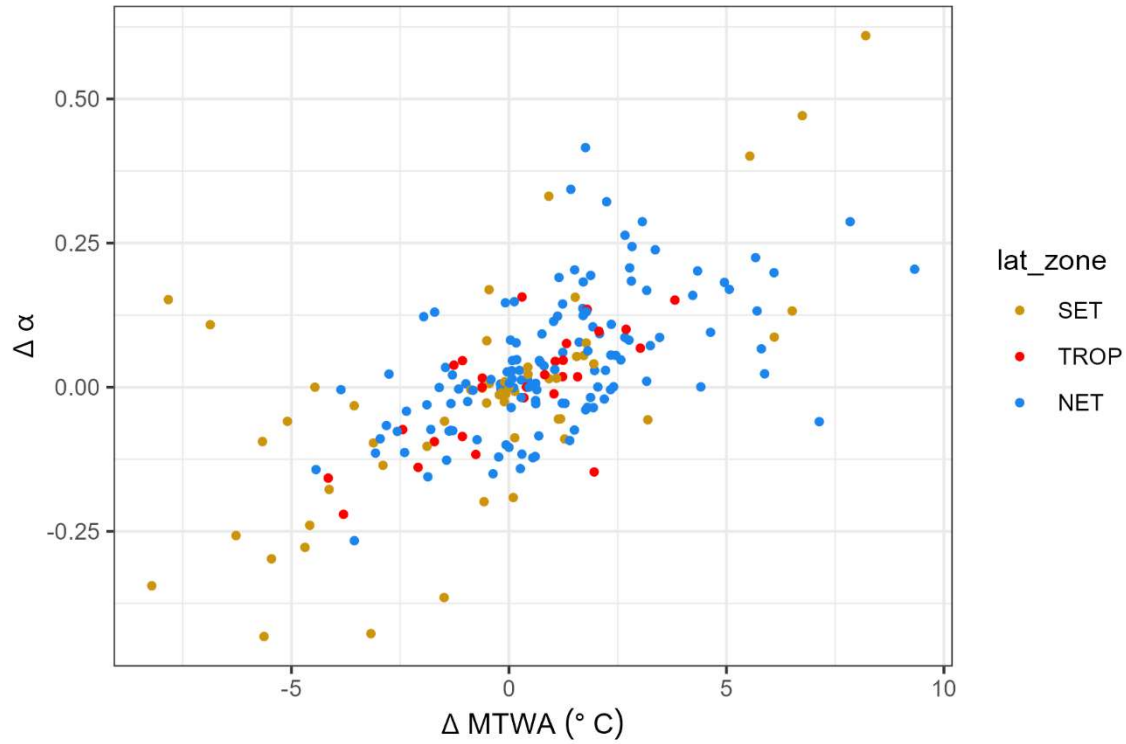
606 Figure 3: Scatter plot of the change in mean temperature of the coldest month (ΔMTCO) versus
607 the change in mean temperature of the warmest month (ΔMTWA) during individual
608 Dansgaard-Oeschger (D-O) events at individual sites. The points are colour-coded to indicate
609 whether the sites are from the northern extratropics (NET, north of 23.5°N), the tropics (TROP,
610 between 23.5°N and 23.5°S) or southern extratropics (SET, south of 23.5°S).



611

612

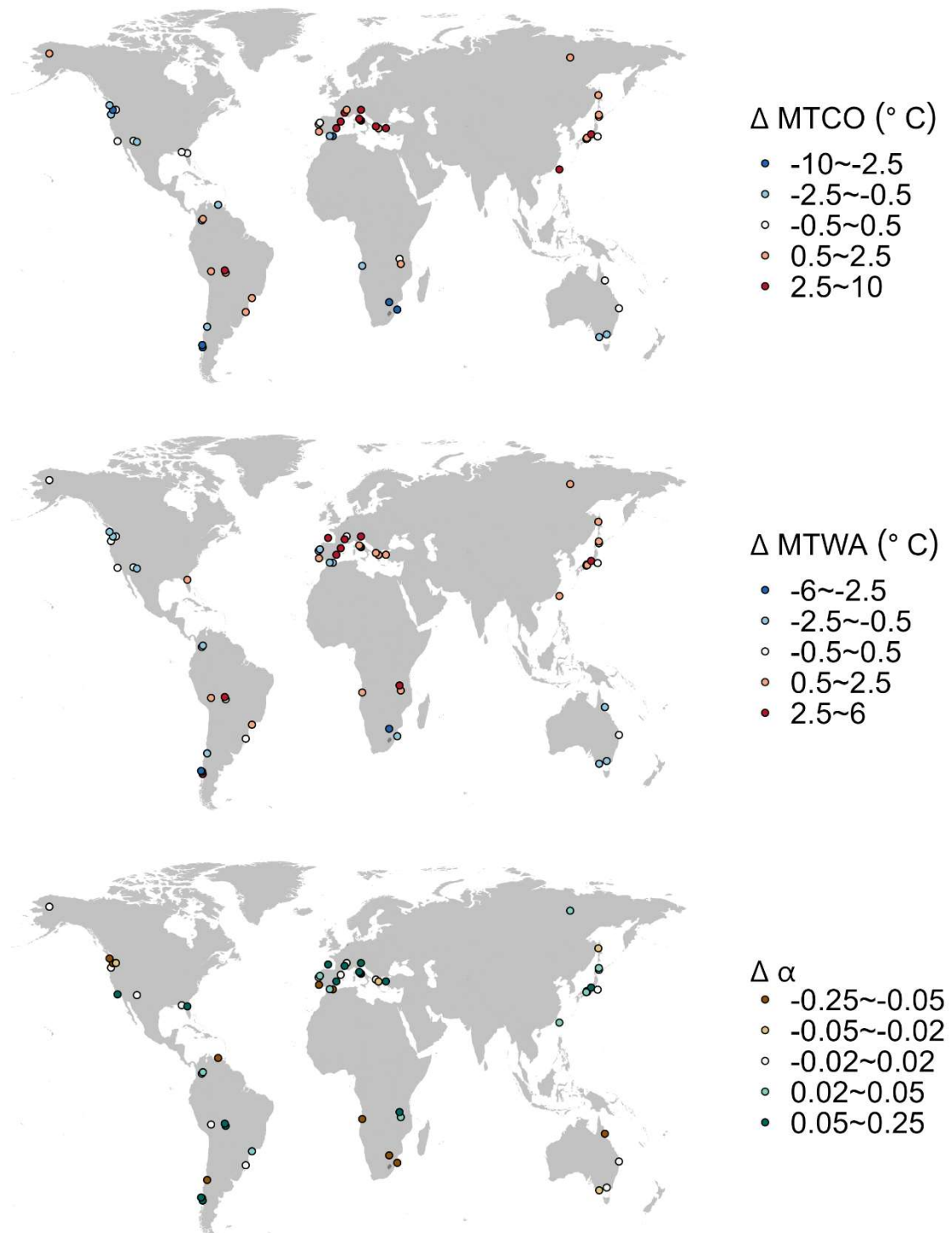
613 Figure 4: Scatter plot of the change in plant-available moisture ($\Delta\alpha$) versus the change in mean
614 temperature of the warmest month (ΔMTWA) during individual Dansgaard-Oeschger (D-O)
615 events at individual sites. The points are colour-coded to indicate whether the sites are from
616 the northern extratropics (NET, north of 23.5°N), the tropics (TROP, between 23.5°N and
617 23.5°S) or southern extratropics (SET, south of 23.5°S).



618

619

620 Figure 5: Maps showing the median change of site-based reconstructions for Dansgaard-
 621 Oeschger (D-O) events 5~12.



622

623

624 Table 1: Details of the sites from the Abrupt Climate Changes and Environmental Responses
 625 (ACER) database (Sánchez Goñi et al., 2017) covering the interval between 50 ka and 30 ka
 626 used for the climate reconstructions. n_{due} is the number of D-O events that should be found
 627 based on the time interval covered by the record. n_{miss} is the number of D-O events that were
 628 not identified. n_{low} is the number of D-O events missed because of low resolution of part of the
 629 record. Some of the 73 sites (indicated by NA in n_{due} , n_{miss} and n_{low}) provide records for parts
 630 of the 50-30ka interval but not for the intervals of the D-O events. Reconstructions based on
 631 samples where the D-O signal was not identified were not used in subsequent analyses. The
 632 full citations for each site are given in Supplementary Materials.

Site name	Latitude	Longitude	Elevation (m)	Site type	Reference(s)	n_{due}	n_{miss}	n_{low}
Abric Romani	41.53	1.68	350	TERR	Burjachs & Julià (1994)	2	0	0
Azzano Decimo	45.8833	12.7165	10	TERR	Pini et al. (2009)	6	2	2
Caledonia Fen	-37.3333	146.7333	1280	TERR	Kershaw et al. (2007b)	8	0	0
Cambara do Sul	-29.05	-50.1	1040	TERR	Behling et al. (2004)	7	0	0
Camel Lake	30.26	-85.01	20	TERR	Watts et al. (1992)	2	1	1
Carp Lake	45.91	-120.88	720	TERR	Whitlock and Bartlein (1997); Whitlock et al. (2000)	8	1	1
Colônia	-23.87	-46.71	900	TERR	Ledru et al. (2009)	7	2	2
Core Trident 163 31B	-3.61	-83.96	-3210	MARI	Heusser and Shackleton (1994)	NA	NA	NA
Fargher Lake	45.88	-122.58	200	TERR	Grigg and Whitlock (2002)	8	2	1
Fundo Nueva	-41.28	-73.83	66	TERR	Heusser et al. (2000)	6	1	0
Fuquene	5.45	-73.46	2540	TERR	van Geel and van der Hammen (1973); Mommersteeg (1998)	7	3	3
Füramoos	47.98	9.88	662	TERR	Müller et al. (2003)	NA	NA	NA
GeoB3104	-3.67	-37.72	-767	MARI	Behling et al. (2000)	NA	NA	NA
Hay Lake	34	-109.425	2780	TERR	Jacobs (1985)	5	3	3
Ioannina	39.75	20.85	470	TERR	Tzedakis et al. (2002); Tzedakis et al. (2004)	8	1	0
Joe Lake	66.76667	-157.217	183	TERR	Anderson (1988); Anderson et al. (1994)	7	3	3
Kalaloch	47.6053	-124.371	19	TERR	Heusser (1972)	8	1	0
Kamiyoshi Basin (KY01)	35.102	135.586	335	TERR	Takahara et al. (2000);; Takahara et al. (2007); Hayashi et al. (2009)	2	0	0
Kashiru Bog	-3.47	29.57	2240	TERR	Bonnefille & Riollet (1988); Bonnefille et al. (1992)	2	2	2
Kenbuchi Basin	44.05	142.383	135	TERR	Igarashi et al. (1993); Igarashi (1996)	3	0	0
Khoe	51.341	142.14	15	TERR	Igarashi et al. (2002)	6	2	2
Kohuora	-36.95	174.8667	5	TERR	Newnham et al. (2007)	NA	NA	NA
Kurota Lowland	35.517	135.879	20	TERR	Takahara & Kitagawa (2000)	3	0	0
KW31	3.52	5.57	-1181	MARI	Lézine & Cazet (2005);	NA	NA	NA

					Lézine et al. (2005)			
La Laguna	4.92	-74.03	2900	TERR	Helmens et al., 1(1996)	2	0	0
Lac du Bouchet	44.83	3.82	1200	TERR	Reille and de Beaulieu (1990)	8	0	0
Lagaccione	42.57	11.8	355	TERR	Magri (1999); Magri (2008)	7	0	0
Laguna Bella Vista	-13.6167	-61.55	600	TERR	Burbridge et al. (2004)	2	0	0
Laguna Chaplin	-14.4667	-61.0667	600	TERR	Burbridge et al. (2004)	3	0	0
Lake Billyakh	65.2833	126.7833	340	TERR	Müller et al. (2010)	4	0	0
Lake Biwa (BIW95-4)	35.245	136.054	84	TERR	Takemura et al. (2000); Hayashida et al. (2007); Hayashi et al. (2010)	3	0	0
Lake Consuelo (CON1)	-13.95	-68.991	1360	TERR	Urrego et al. (2005); Urrego et al. (2010)	7	0	0
Lake Malawi	-11.22	34.42	470	TERR	DeBusk (1998)	6	1	1
Lake Masoko	-9.33	33.75	840	TERR	Vincens et al. (2007)	2	0	0
Lake Nojiri	36.831	138.216	657	TERR	Kumon et al. (2009)	8	0	0
Lake Tulane	29.83	-81.95	36	TERR	Grimm et al. (1993); Grimm et al. (2006)	8	2	2
Lake Wangoom LW87 core	-38.35	142.6	100	TERR	Harle et al. (2002)	7	1	1
Lake Xinias	39.05	22.27	500	TERR	Bottema (1979)	8	3	3
Les Echets G	45.9	4.93	267	TERR	de Beaulieu & Reille (1984)	8	1	0
Little Lake	44.16	-123.58	217	TERR	Grigg et al. (2001)	5	0	0
Lynchs Crater	-17.3667	145.7	760	TERR	Kershaw et al. (2007a)	8	1	1
MD01-2421	36.02	141.77	-2224	MARI	Igarashi & Oba (2006); Oba et al. (2006); Aoki et al. (2008)	8	0	0
MD03-2622 Cariaco Basin	10.7061	-65.1691	-877	MARI	González et al. (2008); González and Dupont (2009)	3	0	0
MD04-2845	45.35	-5.22	-4100	MARI	Sánchez Goñi et al. (2008); Daniau et al. (2009)	2	0	0
MD84-629	32.07	34.35	-745	MARI	Cheddadi & Rossignol-Strick (1995)	NA	NA	NA
MD95-2039	40.58	-10.35	-3381	MARI	Roucoux et al. (2001); Roucoux et al. (2005)	5	0	0
MD95-2042	37.8	-10.17	-3148	MARI	Sánchez Goñi et al. (1999); Sánchez Goñi et al. (2000); Daniau et al. (2007); Sánchez Goñi et al. (2008); (Sánchez Goñi et al. (2009)	6	0	0
MD95-2043	36.14	-2.621	-1841	MARI	Sánchez Goñi et al. (2002); Fletcher and Sánchez Goñi (2008)	4	0	0
MD99-2331	41.15	-9.68	-2110	MARI	Sánchez Goñi et al. (2005); Naughton et al. (2007); Sánchez Goñi et al. (2008); Naughton et al. (2009)	5	0	0
Megali Limni	39.1025	26.3208	323	TERR	Margari et al. (2007); Margari et al. (2009)	6	0	0
Mfabeni Peatland	-28.1487	32.51867	11	TERR	Finch & Hill (2008)	5	1	0

Nakafurano	43.367	142.433	173	TERR	Igarashi et al. (1993)	2	0	0
Native Companion Lagoon	-27.68	153.41	20	TERR	Petherick et al. (2008a); Petherick et al. (2008b)	6	0	0
Navarrés	39.1	-0.68	225	TERR	Carrión & van Geel (1999)	3	0	0
ODP 1233 C	-41	-74.45	-838	MARI	Lamy et al. (2004); Heusser et al. (2006)	6	0	0
ODP 820	-16.63	146.3	-280	MARI	Moss & Kershaw (2000); Moss & Kershaw (2007)	NA	NA	NA
ODP site 976	36.2	-4.3	-1108	MARI	Nebout et al. (2002); Masson-Delmotte et al. (2005)	7	0	0
ODP1019	41.66	-124.91	989	MARI	Mix et al. (1999); Pisias et al. (2001)	NA	NA	NA
ODP1078C	-11.92	13.4	-426	MARI	Dupont & Behling (2006); Dupont et al. (2008)	8	0	0
ODP893A	34.28	-120.03	-577	MARI	Heusser (1998); Heusser (2000)	6	0	0
Potato Lake	34.45	-111.33	2222	TERR	Anderson (1993)	4	3	3
Rice Lake (Rice Lake 81)	40.3	-123.22	1100	TERR	L. Heusser, unpublished data	NA	NA	NA
Siberia	-17.09	-64.72	2920	TERR	Mourguiart & Ledru (2003)	1	1	1
Stracciaccappa	42.13	12.32	220	TERR	Giardini (2007)	5	1	1
Tagua Tagua	-34.5	-71.16	200	TERR	Heusser (1990)	6	0	0
Taiquemo	-42.17	-73.6	170	TERR	Heusser et al. (1999); Heusser and Heusser (2006)	8	0	0
Toushe Basin	23.82	120.88	650	TERR	Liew et al. (2006)	8	1	1
Tswaing Crater	-25.4	28.08	1100	TERR	Partridge et al. (1997); Scott et al. (2008); L. Scott, unpublished data;	6	1	1
Tyrrendara Swamp	-38.1986	141.7626	13	TERR	Builth et al. (2008)	NA	NA	NA
Valle di Castiglione	41.9	12.76	44	TERR	Alessio et al. (1986); Follieri et al. (1988); Follieri et al. (1989); Narcisi et al. (1992); Narcisi (1999); Magri & Tzedakis (2000); Magri (2008)	7	2	2
W8709-13 PC	42.11	-125.75	-2712	MARI	Pisias et al. (2001)	NA	NA	NA
W8709-8 PC	42.26	-127.68	-3111	MARI	Heusser (1998); Lyle et al. (1992)	NA	NA	NA
Walker Lake	35.38	-111.71	2500	TERR	Berry et al. (1982); Adam et al. (1985); Hevly (1985)	NA	NA	NA

633

634

635 Table 2: Leave-out cross-validation (with geographically and climatically close sites removed)
636 using fxTWA-PLSv2 for mean temperature of the coldest month (MTCO), mean temperature
637 of the warmest month (MTWA) and plant-available water (α) with P-splines smoothed fx
638 estimation and bins of 0.02, 0.02 and 0.002, respectively. n is the number of components where
639 the last significant number of components is indicated in **bold** (using criteria of $p \leq 0.01$).
640 Avg.bias is the average bias; RMSEP is the root-mean-square error of prediction;
641 and Δ RMSEP is the per cent change of RMSEP, which is $100 \times$
642 $(RMSEP_n - RMSEP_{n-1})/RMSEP_{n-1}$; when $n = 1$, $RMSEP_0$ is the RMSEP of the null
643 model. p assesses whether using the current number of components is significantly different
644 from using one component less. The degree of overall compression is assessed by linear
645 regression of the cross-validated reconstructions on to the climate variable; b_1 and $b_{1.se}$ are the
646 slope and the standard error of the slope, respectively. The closer the slope (b_1) is to 1, the less
647 the compression.

	n	R^2	Avg.bias	RMSEP	Δ RMSEP	p	b_1	$b_{1.se}$
MTCO (°C)	1	0.72	-1.15	6.84	-45.20	0.001	0.83	0.00
	2	0.74	-1.24	6.68	-2.38	0.001	0.84	0.00
	3	0.75	-1.11	6.52	-2.37	0.001	0.85	0.00
	4	0.75	-1.12	6.54	0.33	0.983	0.85	0.00
	5	0.75	-1.14	6.52	-0.29	0.001	0.85	0.00
MTWA (°C)	1	0.50	-0.29	4.00	-27.76	0.001	0.61	0.00
	2	0.60	-0.20	3.62	-9.42	0.001	0.71	0.00
	3	0.60	-0.23	3.58	-1.11	0.001	0.72	0.00
	4	0.60	-0.23	3.58	0.01	0.525	0.71	0.00
	5	0.60	-0.24	3.58	-0.14	0.090	0.71	0.00
α	1	0.61	-0.021	0.191	-37.32	0.001	0.66	0.00
	2	0.62	-0.023	0.189	-0.61	0.001	0.67	0.00
	3	0.63	-0.022	0.187	-1.18	0.001	0.68	0.00
	4	0.64	-0.021	0.184	-1.46	0.001	0.70	0.00
	5	0.64	-0.020	0.184	-0.12	0.002	0.70	0.00
	6	0.64	-0.020	0.184	-0.25	0.001	0.70	0.00
	7	0.65	-0.019	0.183	-0.26	0.001	0.71	0.00
	8	0.65	-0.019	0.183	-0.03	0.255	0.71	0.00
	9	0.65	-0.019	0.183	-0.05	0.121	0.71	0.00
	10	0.65	-0.019	0.183	-0.04	0.130	0.71	0.00

648

649

650 Table 3: Maximum likelihood estimates of the relationship between the change in mean
 651 temperature of the coldest month (ΔMTCO) and the change in mean temperature of the
 652 warmest month (ΔMTWA) by latitudinal bands for the northern extratropics (NET, north of
 653 23.5°N), tropics (TROP, between 23.5°N and 23.5°S) and southern extratropics (SET, south of
 654 23.5°S). The intercepts were set to zero since both variables are changes.

Region		Coefficient	Standard error (SE)	Lower 95%	Upper 95%
NET	Slope	2.135	0.235	1.674	2.596
TROP	Slope	1.385	0.753	-0.091	2.861
SET	Slope	1.809	0.552	0.728	2.891

655

656

657 Table 4: Maximum likelihood estimates of the relationship between the change in plant-
 658 available water ($\Delta\alpha$) and the change in mean temperature of the warmest month (ΔMTWA) by
 659 latitudinal bands for the northern extratropics (NET, north of 23.5°N), tropics (TROP, between
 660 23.5°N and 23.5°S) and southern extratropics (SET, south of 23.5°S). The intercepts were set
 661 to zero since both variables are changes.

Region		Coefficient	Standard error (SE)	Lower 95%	Upper 95%
NET	Slope	0.065	0.009	0.047	0.082
TROP	Slope	0.056	0.009	0.039	0.074
SET	Slope	0.052	0.011	0.031	0.073

662